Designer Binary Nanostructures toward Water Slipping Superhydrophobic Surfaces

Hye-Mi Bok, Tae-Yeon Shin, and Sungho Park*

Department of Chemistry, BK21 School of Chemical Materials Science, and SKKU Advanced Institute of Nanotechnology, Sungkyunkwan University, Suwon 440-746, South Korea

Received October 23, 2007. Revised Manuscript Received December 7, 2007

This report demonstrates a synthetic route for ordering a set of Au nanoparticles on the vertically aligned conducting polymer (polypyrrole) for the superhydrophobic surfaces with low water flow friction. It demonstrates how one can use polymer nanorod pillars and a variety of Au nanoparticles to generate controlled surface roughness. Synthetic strategies utilized to make such surfaces include the electrochemical polymerization of conducting polymers within the confines of anodized alumina templates and subsequent Au nanoparticle immobilization on the surface of polymer pillars. This method provides a surface that contains roughness on two independently controllable levels, say, the submicroscopic roughness from polymer pillar dimensions and the nanoscopic roughness from the appropriate size selection of Au nanoparticles. With the present results, it is clearly evident that a combination of two scale roughnesses composed of nanorods and nanoparticles could be utilized for the synthesis of superhydrophobic surfaces, which mimics the lotus leaves.

1. Introduction

The self-cleaning strategy of the lotus leaves relies on a combination of two scale roughnesses composed of microscale bumps and nanoscale hair-like structures, which are coupled with the leaf's waxy chemical composition to lower the surface energy.[1–3] Contact between such a surface and a water droplet generates repulsive forces that are sufficient to allow the water droplet to form a spherical shape and therefore to roll off the surface. When a water droplet contacts such a surface, it will form a spherical shape whose property is often characterized by a contact angle. Surfaces with very high contact angles typically larger than 150° are called superhydrophobic surfaces.[1–3] The rolling-off of the water droplet and eradicating the contaminants from the leaf are called the lotus effect.[1–4] A lot of research efforts have been devoted to characterizing such structures and therefore mimicking their structures and chemistry to create superhydrophobic surfaces.[5–22] However, other than complicated lithographic approaches, the control of dual roughness is quite limited, and the controllability often relies on the empirical features such as etching, deposition, and drying conditions.[5–22] Herein, we demonstrate how one can use polymer nanorod pillars and a variety of Au nanoparticles (NPs) to generate controlled surface roughness. Synthetic strategies utilized to make such surfaces include the electrochemical polymerization of conducting polymers within the confines of anodized alumina templates and subsequent metal NP immobilization on the surface of polymer pillars. This method provides a surface that contains roughness on two independently controllable levels, say, the submicroscopic roughness from polymer pillar dimensions and the nanoscopic roughness from the appropriate size selection of metal NPs.

2. Experimental Section

The synthesis of vertical arrays of polypyrrole (Ppy) nanorods is based on the anodized alumina template-assisted electrochemical polymerization method, previously utilized by our examples.[23] Briefly, a thin layer of gold (~1 μm) was thermally evaporated on

* Corresponding author. E-mail: spark72@skku.edu. Fax: 82-31-290-7075.

(1) Li, X.-M.; Reinhoudt, D.; Crego-Calama, M. *Chem. Soc. Rev.* **2007**, *36*, 1350.
(2) Feng, X.; Jiang, L. *Adv. Mater.* **2006**, *18*, 3063.
(3) Feng, L.; Li, S. H.; Li, Y. S.; Li, H. J.; Zhang, L. J.; Zhai, J.; Song, Y. L.; Liu, B. Q.; Jiang, L.; Zhu, D. B. *Adv. Mater.* **2002**, *14*, 1857.
(4) Sung, T.; Feng, L.; Gao, X.; Jiang, L. *Acc. Chem. Res.* **2005**, *38*, 644.
(5) Larmour, I. A.; Bell, S. E. J.; Saunders, G. C. *Angew. Chem., Int. Ed.* **2007**, *46*, 1710.
(6) Lim, H. S.; Han, J. T.; Kwak, D.; Jin, M.; Cho, K. *J. Am. Chem. Soc.* **2006**, *128*, 14458.
(7) Bormashenko, D.; Stein, T.; Whyman, G.; Bormashenko, Y.; Pogreb, R. *Langmuir* **2006**, *22*, 9982.
(8) Pacifico, J.; Endo, K.; Morgan, S.; Mulvaney, P. *Langmuir* **2006**, *22*, 11072.
(9) Cho, W. K.; Kang, S. M.; Kim, D. J.; Yang, S. H.; Choi, I. S. *Langmuir* **2006**, *22*, 11208.
(10) Zhang, L.; Zhou, Z.; Cheng, B.; Desimone, J. M.; Samulski, E. T. *Langmuir* **2006**, *22*, 8576.
(11) Shi, F.; Song, Y.; Niu, J.; Xia, X.; Wang, Z.; Zhang, X. *Chem. Mater.* **2006**, *18*, 1365.
(12) Artus, G. R. J.; Jung, S.; Zimmermann, J.; Gautschi, H.-P.; Marquardt, K.; Seeger, S. *Adv. Mater.* **2006**, *18*, 2758.
(13) Chen, H.; Zhang, F.; Fu, S.; Duan, X. *Adv. Mater.* **2006**, *18*, 3089.
(14) Abdelsalam, M. E.; Bartlett, P. N.; Kelf, T.; Baumberg, J. *Langmuir* **2005**, *21*, 1753.
(15) Xu, L.; Chen, W.; Mulchandani, A.; Yan, Y. *Angew. Chem., Int. Ed.* **2005**, *44*, 6009.
(16) Li, Y.; Shi, G. *J. Phys. Chem. B* **2005**, *109*, 23787.
(17) Shirtcliffe, N. J.; McHale, G.; Newton, M. I.; Chabrol, G.; Perry, C. C. *Adv. Mater.* **2004**, *16*, 1929.
(18) Martines, E.; Seunarine, K.; Morgan, H.; Gadegaard, N.; Wilkinson, C. D. W.; Riehle, M. O. *Nano Lett.* **2005**, *5*, 2097.
(19) Erbil, H. Y.; Demirel, A. L.; Mert, Y. A. O. *Science* **2003**, *299*, 1377.
(20) Callies, M.; Quere, D. *Soft Matter* **2005**, *1*, 55.
(21) Yu, X.; Wang, Z.; Jiang, Y.; Shi, F.; Zhang, Z. *Adv. Mater.* **2005**, *17*, 1289.

10.1021/cm703038j CCC: $40.75
Published on Web 02/20/2008

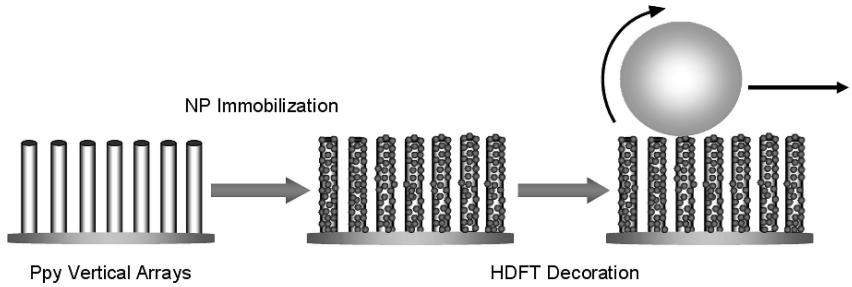

Figure 1. Schematic of the experimental procedure for the synthesis of vertically aligned smooth Ppy nanorod arrays with Au NPs. After spontaneous Au NP decoration, the surface of the NPs was coated with HDFT by immersing in 0.01 M HDFT toluene solution for 12 h.

one side of a nanoporous anodized alumina membrane (pore size = 250−350 nm) and served as a working electrode in a three-electrode electrochemical cell after making physical contact with a glassy carbon electrode. Pt wire and a Ag/AgCl electrode were employed as counter and reference electrodes respectively. Next, Ppy nanorods were electrochemically grown in the interior of an anodized alumina template at constant potential, +1.0 V vs Ag/AgCl, by using a monomer solution (0.5 M pyrrole with 0.2 M tetraethylammonium tetrafluoroborate in acetonitrile). The Ppy length was controlled by monitoring the total charge passed through the cell. A total charge of 0.5 C/cm^2 was passed through for Ppy $L \sim 1.3$ μm, 1.0 C/cm^2 for approximately 5.7 μm, and 1.5 C/cm^2 for approximately 9.7 μm, respectively. It took typically within 10 min for the synthesis. The AAO template (from Whatman International) was dissolved with 3 M sodium hydroxide solution and then repeatedly rinsed with distilled water.

For Au NP synthesis, all the chemicals were obtained from Aldrich and were used as received. The Au colloid sol ($d = 13.6 \pm 1.4$ nm) was synthesized by the following procedures. A volume of 5 mL of 20.0 mM aqueous $HAuCl_4 \cdot 3H_2O$ solution was added to 200 mL of triply deionized water (Millipore), which was then boiled. A volume of 10 mL of 38.8 mM sodium citrate was added to the solution, which was then boiled for 20 min. For the small Au colloid sol ($d = 4.3 \pm 0.5$ nm), 1.25 mL of 20.0 mM aqueous $HAuCl_4 \cdot 3H_2O$ solution was added to 100 mL of triply deionized water. To this solution, 0.0147 g of sodium citrate was added, and subsequently 3.0 mL of 0.1 M sodium borohydride ($NaBH_4$) was added with vigorous stirring for 60 min. For the large Au colloid sol ($d = 49.6 \pm 4.1$ nm), the seed-mediated-growth method was used. A volume of 4 mL of 20 mM aqueous $HAuCl_4 \cdot 3H_2O$ solution and a volume of 0.4 mL of 10 mM $AgNO_3$ solution were added to 170 mL of triply deionized water. Then, 5 mL of aforementioned 13 nm Au NP sol was added to the solution. While stirring, 30 mL of 5.3 mM ascorbic acid was added slowly (0.6 mL/min). For the Au colloid sol ($d = 84.1 \pm 6.0$ nm), a similar procedure as one for the Au colloid sol ($d = 49.6 \pm 4.1$ nm) was used except for the different amount of 13 nm seed Au NP sol, say, 1 mL. The average particle diameters were determined by field-emission scanning electron microscopy (FESEM) images, counting 60 particles. Transmission electron microscopy (TEM) images were used (JEOL JEM-3011) to determine the size of small Au NPs ($d = 4.3 \pm 0.5$ nm).

The surface of the binary nanostructures (Ppy rods and Au NPs) was coated with heptadecafluoro-1-decanethiol (HDFT) by immersing in 0.01 M toluene solution for 12 h, to lower the surface energy for superhydrophobic surfaces.

The morphology of the resulting nanorods was investigated by a field emission scanning electron microscope JEOL 7000F. The water contact angles on such surfaces were measured using the SEO 300A at ambient temperature. The sliding angle movie clips were obtained by a Canon IXY 600 digital camera. All the measurements were performed five times, and the average values with corresponding standard deviations were obtained.

3. Results and Discussion

Figure 1 shows a schematic diagram of the steps involved in preparing the vertical Ppy nanorod arrays decorated with Au NPs. The length of polymer nanorod can be controlled by monitoring the charge passed during the electrochemical polymerization process. The surface of Ppy nanorods is positively charged at pH ~ 6 because the polymer is oxidized and the lone-pair electrons at nitrogen can be protonated under such conditions (pK_a of pyrrole in water ~ 15). The subsequent exposure of the nanorod arrays to a suspension of citrate-stabilized colloidal Au NPs whose surfaces are negatively charged (zeta potential ~ −44.2 mV) could lead to the spontaneous decoration of such nanorod surfaces with Au NPs. The electrostatic interaction between the positively charged Ppy surface and the negatively charged Au NP is the driving force for the spontaneous immobilization of Au NPs. When the similar experiment was carried out with positively charged Au NPs (zeta potential ~ +40.5 mV) as control experiments, there was no NP immobilization. This is further evidence that the NP immobilization is induced by electrostatic interactions. The immobilized Au NPs maintain a certain amount of charge, and the repulsive interparticle interactions prevent additional particle immobilization on top of the immobilized ones.[24] Consequently, it forms the two-dimensional (2-D) arrays of Au NPs rather than three-dimensional clusters, in which most particles are not in direct contact with each other at the saturation limit.

Their immobilization kinetics is different from that in the case with functionalized flat surfaces. On a flat surface, the whole surface is evenly decorated with Au NPs as a function of immersion time and their adsorption kinetics followed the square root of immersion time.[25] The longer the immersion time is, the more immobilized NPs on the surface. However, the immobilization of Au NPs on the vertical arrays of the Ppy nanorods revealed the different adsorption behaviors, as shown in Figure 2. At a very early point, only tips of polymer nanorods are decorated with Au NPs with very few

(22) Zhou, Y.; Yi, T.; Li, T.; Zhou, Z.; Li, F.; Huang, W.; Huang, C. *Chem. Mater.* **2006**, *18*, 2974.
(23) Park, S.; Lim, J.-H.; Chung, S.-W.; Mirkin, C. A. *Science* **2004**, *303*, 348.
(24) Grabar, K. C.; Freeman, R. G.; Hommer, M. B.; Natan, M. J. *Anal. Chem.* **1995**, *67*, 735.
(25) Grabar, K. C.; Smith, P. C.; Musick, M. D.; Davis, J. A.; Walter, D. G.; Jackson, M. A.; Guthrie, A. P.; Natan, M. J. *J. Am. Chem. Soc.* **1996**, *118*, 1148.

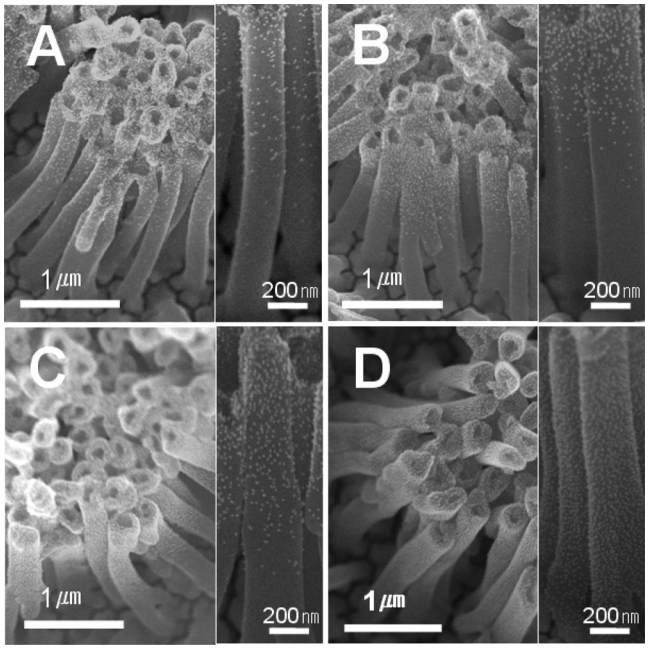

Figure 2. FESEM images of Ppy nanorod arrays with different immersion times in Au NP solutions ($d \approx 13.6$ nm), for (A) 4, (B) 6, (C) 8, and (D) 12 h. Right-hand side insets show the corresponding zoom-in side views.

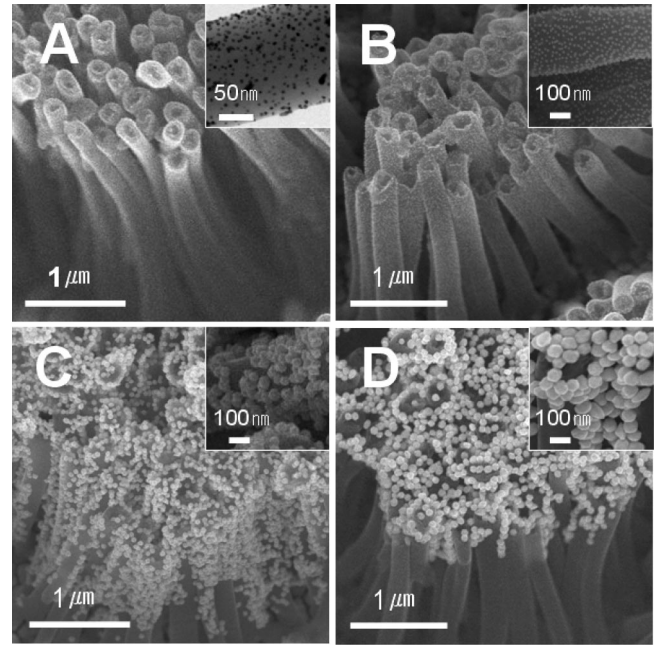

Figure 3. FESEM images of Ppy nanorod arrays with different sizes of Au NPs, (A) 4.3 (±0.5), (B) 13.6 (±1.4), (C) 49.6 (±4.1), and (D) 84.1 (±6.0) nm, respectively. The immersion time was 24 h for all the samples. Insets (B, C, and D) show the zoom-in FESEM images of the corresponding images. The inset of A is the TEM image.

NPs on the side of nanorods. As the immersion time increases, the density of immobilized Au NPs increases from the top to the bottom of the nanorods. At the early stage, the collision probability of Au NPs toward the tip is much higher than the side of the nanorod. After forming a saturate coverage on the tip, the repulsive interaction among NPs prevents the additional immobilization of NPs on the previously immobilized NPs. Then, the NPs can diffuse into the matrix of polymer nanorod arrays and it leads to the gradual saturation of Au NPs from the top part of the nanorod structures. By controlling the exposure time, arrays can be obtained with different densities of NPs from the tip to the bottom of the nanorods. This immobilization scheme is very general and can be applied to colloidal Au NPs with any diameter. We tested a variety of Au NP sizes. As evident in Figure 3A−D, the FESEM images show a set of NP decorated polymer arrays, with NP diameters, 4.3 (±0.5), 13.6 (±1.4), 49.6 (±4.1), and 84.1 (±6.0) nm, respectively. The immersion time was 24 h for all the samples. As clearly evident, when the NP size becomes larger, the interparticle mean distance is altered to be closer. Obviously, when the diameter of the NPs is comparable to the internanorod distance, the NPs cannot effectively diffuse into the open space between nanorods, and therefore the immobilization occurs mainly on the upper part of the nanorod arrays.

The focus here is on the factors that govern the surface wettability and the water slipping angles. The resulting binary nanostructures allow us to systematically control the dual roughness factors by tailoring the nanorod length and NP size. A series of binary nanostructures synthesized via the scheme in Figure 1 are represented in Figure 4 with both their corresponding rod and particle sizes and the measured contact angles. As a control experiment, the contact angle measurements on flat glass surfaces (i.e., the length of Ppy rod ∼ zero) are also represented in the second column. The

Au NP size \ Ppy length	Without Ppy	1.3 μm (±0.1 μm)	5.7 μm (±0.2 μm)	9.8 μm (±0.3 μm)
Without Au NPs		12 ± 2°	7 ± 1°	3 ± 1°
4.3 nm (±0.5 nm)	99 ± 1°	143 ± 3°	149 ± 3°	158 ± 2°
13.6 nm (±1.4 nm)	108 ± 2°	148 ± 3°	158 ± 2°	160 ± 3°
49.6 nm (±4.1 nm)	119 ± 2°	152 ± 1°	161 ± 4°	165 ± 2°
84.1 nm (±6.0 nm)	132 ± 1°	147 ± 2°	151 ± 2°	160 ± 4°

Figure 4. Contact angle measurements with a series of Ppy nanorods and Au NPs after HDFT coating. The contact angles were measured with a water droplet of 3 μL, and their corresponding contact angle values are described with specific numbers. Au NP size represents the diameter (d). The substrate is a glass slide.

2-D Au NP arrays on flat surfaces are prepared by following the previous reports.[26,27] Their corresponding FESEM images are represented in Figure 5. As expected, the surface roughness varies as a function of NP sizes. Their contact angles were measured with a water droplet (3.0 μL). The larger NP film showed the higher contact angles due to the

(26) Reincke, F.; Hickey, S. G.; Kegel, W. K.; Vanmaekelbergh, D. *Angew. Chem., Int. Ed.* **2004**, *43*, 458.
(27) Li, Y.-J.; Huang, W.-J.; Sun, S.-G. *Angew. Chem., Int. Ed.* **2006**, *45*, 2537.

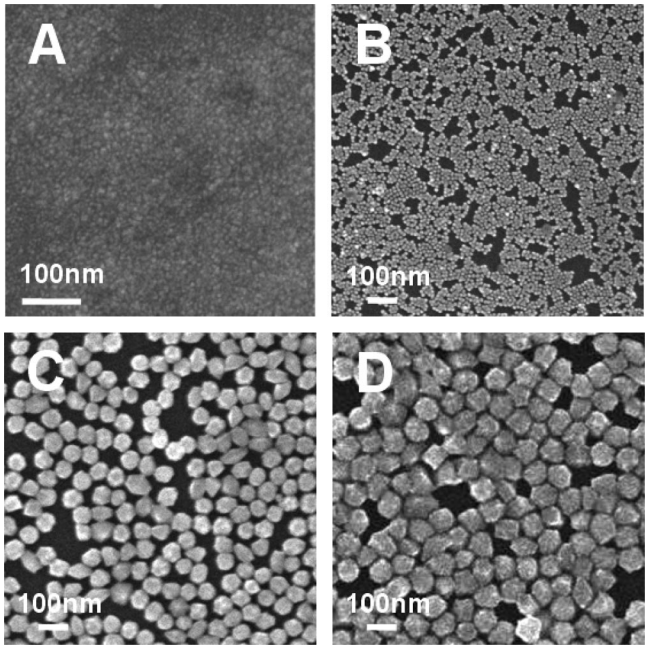

Figure 5. FESEM images of monolayer Au NP films on silicon wafer. The sizes (d) of used Au NPs are (A) 4.3 (±0.5) nm, (B) 13.6 (±1.4) nm, (C) 49.6 (±4.1) nm, and (D) 84.1 (±6.0) nm.

increase of surface roughness, as shown in Figure 4, second column.

The roughness-dependent contact angle variation can be understood by the Wenzel model, in which there is a linear relationship between the apparent contact angle and the roughness factor of the surface. It is represented by a simple equation $\cos \Theta_w = r \cos \Theta$, where Θ_w represents the apparent contact angle, r corresponds to the surface roughness factor, and Θ is the intrinsic contact angle.[28] This model states that if Θ on a smooth surface is more than 90°, the Θ_w will become larger as the roughness increases. This roughness factor (r) increases as the particle size increases in our system. This trend is clearly evident in our 2-D NP arrays on flat surfaces. However, it was not feasible to obtain a superhydrophobic ($\Theta_w > 150°$) surface with a nanoscopic roughness level endowed solely by NP arrays. When the NPs were immobilized on the vertical arrays of polymer pillars, the contact angles dramatically increased. As clearly evident in Figure 4, there are two noticeable features. First, the hydrophobicity increases as the rod length increases for the fixed size of the NPs. For the NP diameter ($d \approx 4.3$ nm), the contact angle on a flat surface ($\Theta_w \approx 99°$) increased to the value $\Theta_w \approx 143°$ on the polymer pillar arrays ($L \approx 1.3$ μm). This value was further monotonically enhanced as the polymer pillar length increased, as exhibited in the third row of Figure 4. This trend is consistent with any diameter of NPs. Second, for a given nanorod length, the dewettability was affected by the size of NPs immobilized on the surface of the nanorods. For instance, the last column shows the consistent increase of contact angles from 158° to 160° and 165°, when the immobilized NP sizes are 4.3, 13.6, and 49.6 nm, respectively. However, one noticeable feature is that this value shows the maximum point with 49.6 nm NPs and starts to decrease again to 160° when the size of the NPs is approximately 84.1 nm. This is clearly different from the case with flat surfaces (in the second column in Figure 4). Obviously, the control of dual roughness plays a critical roll in fine-tuning the contact angles. Significantly, the results show that the double roughness architecture helps in amplifying the apparent contact angle, which is consistent with Patankar's recent theoretical analysis.[29] According to his analysis, the double roughness also enhances water slippage on such structures because of the easy formation of composite drop with favorable energy state. The contact angle of composite water droplets can be described by the Cassie−Baxter (CB) model, which states that the apparent contact angle is the sum of all the contributions of different phases, saying $\cos \Theta_c = f(1 + \cos\Theta) - 1$, where Θ_c represents the apparent contact angle, and f and Θ correspond to the surface fraction of solid/water and the intrinsic contact angle on the smooth solid surface, respectively.[30] Therefore, the smaller the surface solid fraction is, the larger the apparent contact angle (Θ_c) results.

Both the Wenzel and the CB models can explain the contact angle enhancement with the increase of nanorod lengths, due to the roughness increase or air entrapment below the water droplet, respectively. However, the decrease of contact angles on the given polymer nanorod length with large NPs ($d \approx 84.1$ nm) cannot be explained by the Wenzel model. As shown in the second column, the increase of contact angles on the flat surfaces is attributed to the roughness increase as the NP size increased. The roughness increase with polymer pillars is also clear. However, the 49.6 nm NPs showed the maximum contact angles for all the investigated binary nanostructures with polymer pillars. This observation reveals that the nanoscopic roughness is critical for the air entrapment. We believe that the 3-D arrays of 49.6 nm Au NPs with polymer pillars are better than 13.6 and 84.1 nm NPs in terms of air trapping. In contrast to the case with flat surfaces, if the air entrapping played an important roll in the augmentation of contact angles with the binary nanostructures, the water droplet slippage with low surface friction would be observed with different characteristics. Usually, the contact angle hysteresis which is the angle difference between advancing and receding contact angles is often used to differentiate the two models. In the CB model, the contact angle hysteresis is extremely small, but this value becomes large in the Wenzel one. In the CB model, the low surface energy of air reduces the friction force when a water droplet moves. However, the opposite trend is the resulting phenomenon in the Wenzel model, which favors water droplet pinning and therefore leads to the increase of friction force. Therefore, the sliding angle measurement is critical in terms of differentiating the two models. When the contact angle hysteresis becomes smaller, the sliding angle of a water droplet shows smaller values, which follows the CB model. The quantitative relationship between the contact angle hysteresis and the sliding angle is given by Furmidge, say, $mg \sin \alpha = \gamma w(\cos \Theta_R - \cos \Theta_A)$, where α is the sliding angle, mg is the weight

(28) Wenzel, R. N. *Ind. Eng. Chem.* **1936**, *28*, 988.

(29) Patankar, N. A. *Langmuir* **2004**, *20*, 8209.

(30) Cassie, A. B. D.; Baxter, S. *Trans. Faraday Soc.* **1944**, *40*, 546.

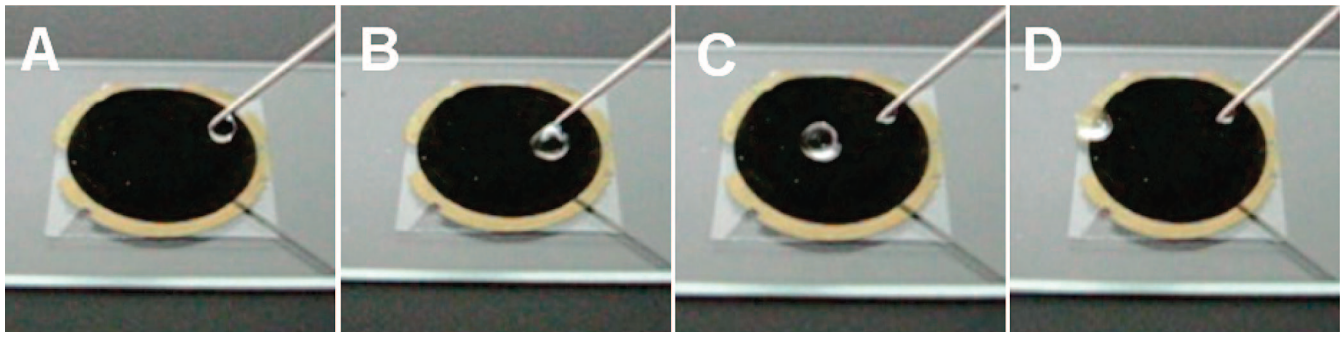

Figure 6. (A−D) Snapshot photographs of a water droplet (10 μL) on binary nanostructures, with Ppy ($L \approx 9.8$ μm) and NPs ($d \approx 49.6$ nm). It took ca. 0.2 s from A to D. The titling angle is ca. 2°. The corresponding contact angle is described in the Figure 4 (the fifth column and the fifth row). The diameter of substrates is approximately 2 cm.

of the water droplet, w is the diameter of the wetted area, γ is the interfacial tension of the water at the water/air interface, and Θ_R and Θ_A are the receding and the advancing contact angles.[31] From this relationship, it can be found that a smaller difference between the advancing and the receding contact angles will lead to a smaller sliding angle (α). We measured the sliding angles for all the samples and found that the 2-D arrays of NPs on the flat surfaces represented very high sliding angles, typically >90° for 10 μL water droplets (Supporting Information, Movie Clip 1). Even the upturned tilting showed the strong sticking characteristics of water droplets on such surfaces. Therefore, the second column in Figure 4 clearly resulted from the roughness increase with NP size increase, which is accountable with the Wenzel model. However, all the investigated binary nanostructures showed very low sliding angles, typically <2° (Supporting Information, Movie Clip 2). In a typical experiment, the binary nanostructure (Ppy $L \approx 9.8$ μm and NP $d \approx 49.6$ nm) shows a water droplet rolling off on such surfaces with a tilting angle of approximately 2°, as shown in Figure 6. Compared to 2-D NP arrays on the flat surfaces, the binary nanostructure architecture shows enhanced contact angles with very low sliding angles. Obviously the double roughness that the first one is endowed by the controllable length of nanorod arrays and the second one is specified by the selection of appropriate NP sizes increases the apparent contact angle. More importantly, it also enhances water rolling on such surfaces with low friction forces, which is critical for the self-cleaning or lotus effect.

Given that the internanorod distance and the individual rod size can be tuned by the physical dimensions of the template, the controllability of nanorod length and its nanoscopic roughness is another variable where the surface dewettability and water slippage can be further enhanced. There are three controllable parameters for the superhydrophobic surface generation. First, the internanorod distance can be tuned by controlling anodized alumina membrane synthetic conditions. Second, the length of nanorods is tailorable with electrochemical polymerization conditions. Third, the nanoscopic roughness on a nanorod can be tuned by the appropriate selection of NPs. As exemplified with the current study, those parameters are important for the increase of dewettability of water droplets. The fine-tuning of those values will allow us to reach very high contact angles.

4. Conclusions

In conclusion, the present results show that it is important to design binary nanostructures to fine-control double roughness features which not only induce air trapping but also make this state more stable. This is achievable by rationally increasing the roughness factor. Admittedly, the present interpretation of the observed contact angle variation on Au NP-Ppy composite films to each dimension in terms of "Wenzel and Cassie−Baxter models" is only qualitative in nature. Obviously, the more complicated theoretical models are necessary to quantitatively describe the contact angle variation on the hierarchical structures, by considering each local roughness.[32] With the present results, at least it is clearly evident that the combination of two scale roughnesses composed of Ppy nanorods and Au NPs could be utilized for the synthesis of superhydrophobic surfaces, which mimics the lotus leaves. We believe that a comparison of the surface wettability with other binary nanostructures with other shaped nanostructures, such as prisms, cubes, and wires, will provide new insight for highly effective surface modification. The combination of a variety of NPs will bring new applications as exemplified with the current study.

Acknowledgment. This work was supported by the Korea Research Foundation Grant funded by the Korean Government (MOEHRD, KRF-2005-005-J11902, and KRF-C00050) and the Korea Science and Engineering Foundation (R01-2006-000-10426-0-2006).

Supporting Information Available: Contact angle measurements on the bare Au NP films (PDF) and movie clips for water droplet sliding on NP arrays on the flat surface and the Ppy arrays. This material is available free of charge via the Internet at http://pubs.acs.org.

CM703038J

(31) Furmidge, C. G. L. *J. Colloid Interface Sci.* **1962**, *17*, 309.

(32) Herminghaus, S. *Europhys. Lett.* **2000**, *52*, 165.